Journal of Pharmaceutical and Biomedical Analysis 211 (2022) 114597

Contents lists available at ScienceDirect

Journal of Pharmaceutical and Biomedical Analysis

journal homepage: www.elsevier.com/locate/jpba

Optimization of sensing-pad functionalizing strategy toward separative extended-gate FET biosensors for PSA detection

Jiahuan Yu[a,b,1], Guosheng Gao[c,1], Bo Sun[a], Lingyan Liang[a,*], Qiang Shen[c], Yang Zhang[d,*], Hongtao Cao[a,b,**]

[a] Laboratory of Advanced Nano Materials and Devices, Ningbo Institute of Materials Technology and Engineering, Chinese Academy of Sciences, Ningbo 315201, People's Republic of China
[b] Center of Materials Science and Optoelectronics Engineering, University of Chinese Academy of Sciences, Beijing 100049, People's Republic of China
[c] HwaMei Hospital, University of Chinese Academy of Sciences, Ningbo 315010, People's Republic of China
[d] Key Laboratory of Semiconductor Material Sciences, Beijing Key Laboratory of Low Dimensional Semiconductor Materials and Devices, Institute of Semiconductors, Chinese Academy of Sciences, Beijing 100083, People's Republic of China

ARTICLE INFO

Article history:
Received 18 July 2021
Received in revised form 6 January 2022
Accepted 13 January 2022
Available online 15 January 2022

Keywords:
Ion-sensitive field effect transistors
Plug-in-card-type
Portable biosensors
Prostate cancer
Debye volume

ABSTRACT

In this study, separative extended-gate AlGaAs/GaAs high electron mobility transistor (HEMT) biosensor is proposed for prostate-specific antigen (PSA) detection. Zinc oxide nanotetrapods (T-ZnO) with a four-leg structure is introduced onto the sensing pad to form a three-dimensional (3D) and concave detection front. Compared with common plane front, the elaborately-designed-3D and concave detection front can offer more biological modification sites and decrease the Debye volume, resultantly improving both the detection scope and sensitivity. Anti-PSA probes can be fixed at any sites of T-ZnO via a chemical bio-functionalization method, which facilitates better detection performance by comparison with a physical modification scheme. On the other hand, the T-ZnO nanostructures with the four-leg configuration are capable of releasing the stress and erosion effect of the solution on the plane Au film, contributing to a great improvement in the reliability of the biosensors. The optimized biosensors with chemical bio-functionalized T-ZnO detection front demonstrate good linear current/voltage response to label-free PSA target in the concentration range from 5 fg/ml~5 ng/ml and a sensitivity variation ~ 1.3% dec^{-1}.

1. Introduction

Electronic biological detection can be integrated into current electronic manufacturing process and technology, and holds prospect for future miniaturized in-situ applications [1]. Among them, sensor based on field-effect transistor (FET) has been widely investigated due to its potential for miniaturization, label-free and fast response time [2–4]. The ion-sensitive field effect transistor is the earliest solid-state devices for the sensing of ionic activities which can be traced back to 1970 [5,6]. However, the main drawback of the sensor is its long-term performance drift due to its instability in solution and the degradation of its gate insulators [7,8]. In recent years, scientists have come up with a new configuration called separative extended-gate field effect transistor (SEGFET) [9–12]. This configuration divides a biosensor into two core components, the FET and the sensing pad that are isolated from each other in space. The FET would provide high repeatability and stability since it is free from the chemical corrosion/damage of biological solution. In addition, the two core components have great flexibility in their design and fabrication. For example, the sensing pad can be bio-functionalized and delicately designed to be plug-in-card type, a kind of portable configuration like USB (universal serial bus), according to the specific detection task [13,14].

However, although the SEGFET configuration can protect the FET from solution damage, the sensing pad is vulnerable to damage since it is directly facing the chemical/biological environment. This may lead to deterioration of the stability of the sensing pad and even of the biosensor, bringing about noise signals. In addition, further research is still needed to improve the detection performance. For example, the

Abbreviations: ISFET, Ion-sensitive field effect transistor

* Corresponding authors.
** Corresponding author at: Laboratory of Advanced Nano Materials and Devices, Ningbo Institute of Materials Technology and Engineering, Chinese Academy of Sciences, Ningbo 315201, People's Republic of China.
E-mail addresses: lly@nimte.ac.cn (L. Liang), zhang_yang@semi.ac.cn (Y. Zhang), h_cao@nimte.ac.cn (H. Cao).

[1] Jiahuan Yu and Guosheng Gao contributed equally to this work.

https://doi.org/10.1016/j.jpba.2022.114597
0731-7085/

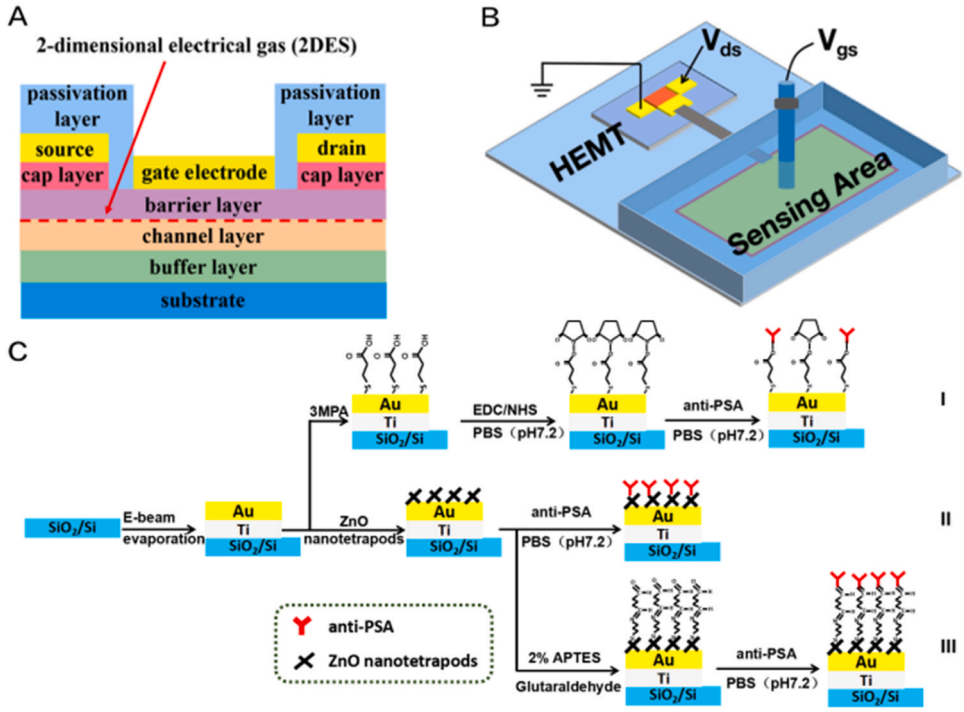

Fig. 1. The structure of HEMT (A) and the corresponding biosensor (B). (C) Three functionalizing strategies of the sensing pads.

sensitivity, a key parameter of FET biosensors, is heavily limited by screening of electric fields by mobile ions in biological solution [15–17]. Fortunately, there were reports that non-plane-structure sensing pad can help decrease the charge screening and improve the sensitivity. For example, Shoorideh and Chui conducted a series of simulations to demonstrate that the detection front with nanowires on it can be more sensitive than planar ones [18]. Gao et al. introduced a surface coating with an almost constant potential to reduce the screening effect and then largely improved the device sensitivity [19,20]. These researches provide a good idea for the sensing pad optimization to further improve the detection performance.

In this work, SEGFET-configuration biosensors are fabricated to detect prostate-specific antigen (PSA) which is considered to be a marker of prostate cancer. High electron mobility transistor (HEMT) is chosen as the FET component due to a lot of advantages such as high transconductance, low noise [21,22], and so on. ZnO nanostructures have been increasingly used in biological nanotechnology due to their unique advantage such as high chemical stability, specific surface area, biocompatibility, high electron communication feature and so on [23,24]. Among them, zinc oxide nanotetrapods (T-ZnO) possessing a special structure with four legs growing in different directions and resembling closely tetrahedral electronic geometry, were advanced in electron transportation [25,26]. Based on this, T-ZnO is introduced on the sensing pad to form a three-dimensional (3D)-structure detection front. Both physical and chemical functionalization methods are used to fix the probe molecules (anti-PSA) onto T-ZnO. The detection performance and reliability of biosensors with or without T-ZnO are compared in detail. It is found that the additive of T-ZnO is in favor of improving both the sensitivity and the reliability of the biosensors.

2. Experiment section

2.1. Fabrication of HEMT biosensor

The structure of HEMT is shown in Fig. 1A. The AlGaAs/GaAs epitaxy-wafer, which consists of 2 μm-GaAs Buffer layer, 12 nm InGaAs channel layer, 28 nm AlGaAs barrier layer and 30 nm cap layer, was deposited by molecular beam epitaxy. In the procedure of HEMT preparation, inductively coupled plasma etching was firstly used to get graphical active layer. After that, in the step of preparing for the source and drain electrode, Ge/Au/Ni/Au metal stack was grown on EPI-wafer by electron beam evaporation (EBE), and then the samples were annealed in N_2 atmosphere at 410 °C for 20 s to form ohmic contact. Ti/Au metal layer was deposited by magnetron sputtering as gate electrode. Afterward, plasma enhanced chemical vapor deposition was used to deposit SiO_2 and SiN passivation layer to isolate the devices from air. Finally, the areas of electrodes were exposed by using reactive ion etching and buffered oxide etch solution. The electrical resistivity of the HEMT was 388.3 ohm/cm and the sheet electron concentration was 1.9×10^{12} cm^{-3} with a mobility of 8.5×10^3 $cm^2V^{-1}s^{-1}$. After the HEMT was prepared, sensing pad was connected with it through a wire to form a HEMT biosensor. As shown in Fig. 1B, both the sensing pad and the reference electrode were immersed in 0.1 × phosphate buffer saline (0.1 × PBS) solution, and the gate voltage (V_{gs}) was applied through the reference electrode to test the transfer curve of the biosensor using different PSA antigen concentrations ([PSA]) under this configuration.

2.2. Modification of sensing pad

The SEGFET configuration provides great convenience to design and fabricate the sensing pad. In this study, three types of sensing pads (marked as I, II and III, as shown in Fig. 1C) were proposed, corresponding to different functionalizing strategies. Before biofunctionalizing, 40 nm Ti (@150 °C) and 60 nm Au (@room temperature, RT) were deposited in sequence by EBE on a SiO_2/Si wafer as the conductive substrate. Then, anti-PSA was fixed on the Au surface to form pad I by conventional chemical modification method [27].

Different from the pad I, the pads II and III were firstly modified with T-ZnO onto the Au surface. Since ZnO has a relative high isoelectric point of 9.5, it is frequently used as the linker for the adsorption of biomolecules [26]. T-ZnO anhydrous ethanol suspension

(30 mg/ml) was spin-coated on the Au surface at 1200 rpm for 40 s, then thermally annealed at 90 °C for 90 s to remove the redundant ethanol. Finally, anti-PSA (50 μg/ml in 0.1 × PBS, at pH 7.2) was dropped directly onto the sensing pad modified with T-ZnO and kept at 4 °C overnight to immobilize the anti-PSA (pad II).

Different from the physical-adsorption method for the preparation of pad II, a chemical functionalization process was adopted for pad III. The T-ZnO-modified substrate was treated with O_2 plasma (100 W) for 10 min to form hydroxyl group, after that 2% (v/v) 3-aminopropyltriethoxysilane (APTES) anhydrous ethanol solution was dipped onto the T-ZnO, waiting for 40 min to make the amino groups adhere to the T-ZnO surface. According to references [28,29], APTES can be fixed on solid surface via hydrolysis-condensation reaction. A thermal treatment (120 °C, 1 h, air ambient) was performed next to wipe off the unconjugated APTES and redundant anhydrous ethanol. Then the pad was immersed into 2.5% (v/v) glutaraldehyde solution to fix aldehyde group on the T-ZnO surface. Finally, the pad added with anti-PSA was kept at 4 °C overnight to make the anti-PSA covalently linked to the T-ZnO surface. To avoid non-specific binding of the corresponding target PSA, one should block the glutaraldehyde without anti-PSA, such as by bovine serum albumin (BSA) [14].

3. Results and discussion

3.1. Sensing pad and biosensor stability

In order to obtain a stable SEGFET biosensor, it is necessary to study the stability of two core components (HEMT and sensor pad). The transfer curve of the HEMT was measured repeatedly, and the measured curves were kept constant, indicating that the HEMT has sound electrical stability (Fig. S1). As another important component of SEGFET, sensing pad is the interaction zone for biological reaction, working in the solution environment for a long time. Therefore, its stability issue needs to be addressed firstly.

Current-voltage (*I-V*) and capacitance-frequency (*C-f*) curves were repeatedly measured for the anti-PSA-modified sensing pads in pure 0.1 ×PBS (bare-Au sensing pad as a control shown in Fig. S2). The resistance and capacitance @ 1 Hz are derived from the measured curves and their variation is used to evaluate the sensing pad stability. Figs. 2A and 2B demonstrate the relative resistance and capacitance changes, i.e.,

$$\Delta R/R_0 = |R - R_0|/R_0 \quad (1)$$

$$\Delta C/C_0 = |C - C_0|/C_0 \quad (2)$$

where R_0 (C_0) and R(C) is the resistance (capacitance) obtained at the first and fifth time, respectively. For each kind of sensing pad, 5 identical samples were prepared and examined. It can be clearly seen that the $\Delta R/R_0$ of pad I is higher than that of pad II and III. The maximum $\Delta R/R_0$ of the pad I, II and III is 19.4%, 1.7% and 2.1%, respectively. Similarly, pad I shows larger $\Delta C/C_0$ (2.0–10.1%) compared with pads II and III (< 2%, shown in Fig. 2B). These results suggest that the sensing-pad stability can be evidently improved by the additive of T-ZnO.

In addition, the performance repeatability of the whole biosensor (the HEMT and the sensing pads system) was also checked in pure 0.1 ×PBS. Herein, the repeatability is evaluated by the threshold voltage (V_{th}) and relative current changes calculated from the transfer curves. As shown in Fig. 2C, the V_{th} change (ΔV_{th}) of biosensor I is generally larger than those of the counterparts. In

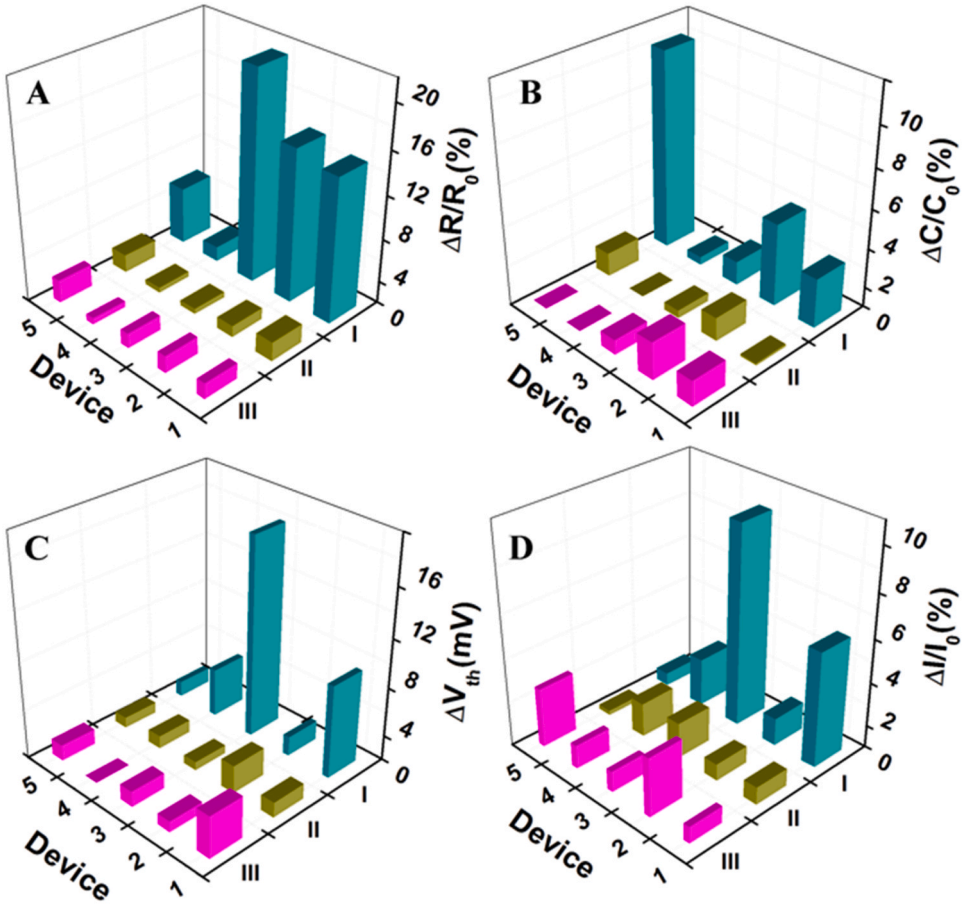

Fig. 2. The $\Delta R/R_0$ (A) and $\Delta C/C_0$ (B) of the pad I, II and III, where five samples are selected for each pad. ΔV_{th} (C) and $\Delta I/I_0$ (D) of the biosensors I, II and III.

Table 1
Comparison of atomic contents of C, N, and N/C at the 5-selected positions.

Sensing pad	position	C atoms percent (%)	N atoms percent (%)	N/C
Bare T-ZnO	a	6.99 ± 0.32	–	–
II	b	10.25 ± 0.50	–	–
	c	15.02 ± 0.69	3.53 ± 0.07	0.24 ± 0.02
III	d	19.06 ± 0.96	3.65 ± 0.32	0.20 ± 0.02
	e	14.16 ± 0.67	3.26 ± 0.29	0.23 ± 0.01

particular, Among the 5 test samples, 80% of biosensors II or III have a ΔV_{th} smaller than 2 mV, while only 40% of biosensors I could have. The maximum ΔV_{th} of biosensors I is even up to 16.4 mV. The relative current changes ($\Delta I/I_0$) of these biosensors are illustrated in Fig. 2D, where the $\Delta I/I_0$ variations are consistent with the ΔV_{th}. Specifically, all of the biosensor II and 80% of biosensor III have a relative current change of less than 2%. However, only 40% of biosensor I can achieve this level (the maximum $\Delta I/I_0$ is up to 9.1%).

3.2. Biosensor detection performance

The ΔV_{th} and sensitivity (S) ,

$$S = |\Delta I/I_0| \times 100\% \quad (3)$$

where ΔI is the change between the I_{ds} in different concentration of analyte and the I_0 in pure PBS, are the common metrics for evaluating the sensor response to analyte [30], which can be extracted from the transfer curves presented in Fig. S3. As displayed in Fig. 3A, the ΔV_{th} fits linearly with the logarithm of the PSA concentrations ([PSA]), yielding a r^2 (r is the correlation factor) of 0.99, 0.98 and 0.95 for the biosensor I, II and III, respectively. The averaged ΔV_{th} for a 10 times concentration variation is about 1.02, 1.93 and 2.57 mV dec^{-1}, corresponding to the biosensor I, II and III, respectively. Based on the abscissa range, the detection scope of the biosensor I is from 50 fg/ml to 50 pg/ml, while that of the biosensor II and III is enlarged to 5 fg/ml~500 pg/ml and 5 fg/ml~5 ng/ml, respectively. The extended detection scope is obtained with the introduction of T-ZnO nanostructures, probably due to the large specific surface area in favor of binding more anti-PSA.

The linear dependence of S on the logarithm of [PSA] is presented in Fig. 3B, with a r^2 of 0.70 (I), 0.90 (II) and 0.99 (III), respectively. The averaged ΔS for a 10 times PSA concentration variation and the S value at 50 pg/ml is 0.5% dec^{-1}, 0.9% dec^{-1}, 1.3% dec^{-1} and 3.6%, 5.7%, 9.4% for the sensor I, II, III, respectively. It should be noted that, due to the poor stability of biosensor I, only one group of reliable data were obtained in our experimental.

3.3. Discussion on the related mechanisms

From the above results, it can be found that both the detection scope and sensitivity of biosensor III is the best, followed by biosensor II and I. And the device reliability are greatly improved by the application of T-ZnO on the sensing pads. It's essential to make clear the underlying mechanisms.

Fig. 4 displays scanning electron microscope (SEM) images of T-ZnO nanostructures, T-ZnO on the pad II and III. The ZnO nanotetrapods have a four-legged structure, a special 3D morphology with high surface area in favor of accommodating more biological markers to boost the detection sensitivity. After all, ZnO has a good biological compatibility [26,31]. After biological modification, however, the legs of T-ZnO were observed to widen, as seen from the SEM images of pads II and III. To analyze the un-known covers, we select 5 typical positions to conduct elemental analysis. The atomic contents of carbon (C) and nitrogen (N) and the N/C atomic ratio are checked and listed in Table 1. The C content in the bare T-ZnO (position a) and the T-ZnO leg tip of pad II (position b) is lower than

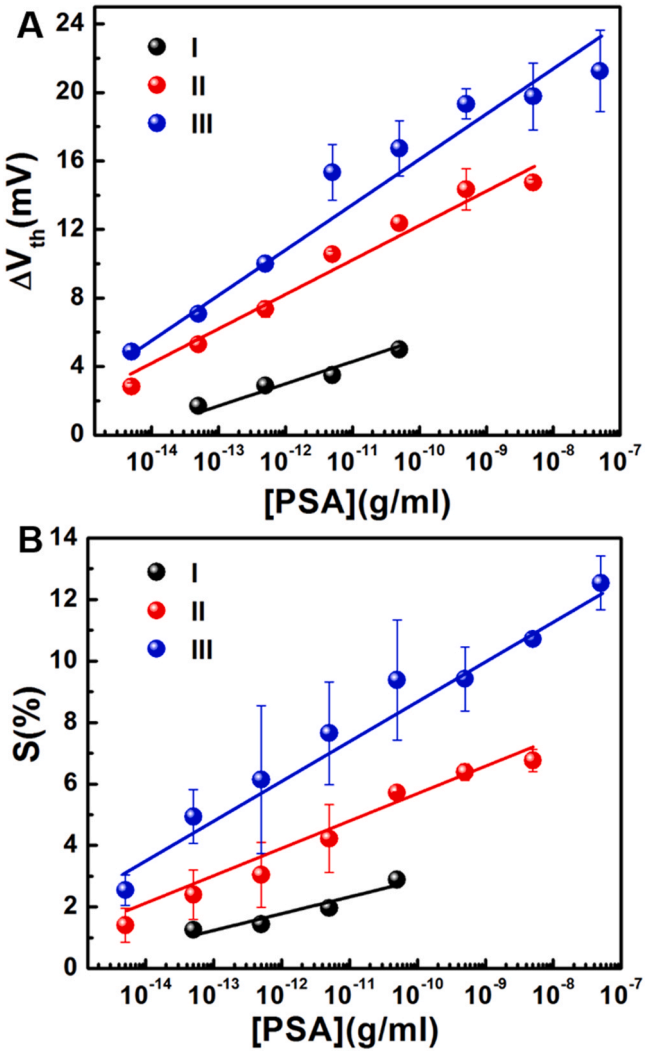

Fig. 3. The ΔV_{th} value (A) and the S (B) for different [PSA] of the biosensor I, II and III in 0.1 × PBS.

those of the other three sites, and the N content of these two sites is too low to be identified (beyond the detection limit). In contrast, intensive C and N signals are detected from the T-ZnO leg bottom of pad II (position c), and the T-ZnO tip (position d)/bottom (position e) of pad III. The C/N ratios of these three sites are very close to each other, implying the same biomolecule located at these positions. In another word, anti-PSA prefers to settle down on the bottom leg of T-ZnO when using the physical functionalization method (pad II), while both the top and bottom leg of T-ZnO can attract the anti-PSA when using the chemical functionalization scheme (pad III). Hence, it can be inferred that the amount of the biological-binding sites available is incremental in a sequence of pad I, II and III. Based on binding kinetics, increasing the concentration of binding sites will shift the equilibrium toward having more PSA bound over a given time period. Therefore, the biosensor III demonstrates the largest detection scope, biosensor II the middle, and biosensor I the smallest.

With regard to the improvement in the detection sensitivity by introducing T-ZnO, it can be explained by the application of 3D detection front which had been reported to be able to decrease the charge screening by constraining the space in which double layers can form [15]. Because this space is filled with counter ions, the screening effect can be weakened by limiting its volume, which is equivalent to increasing the averaged Debye length [15,18]. To help

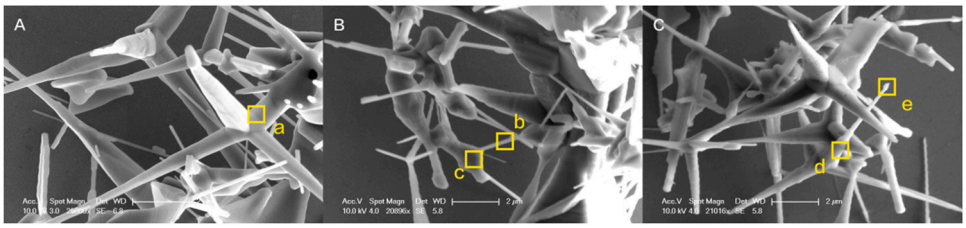

Fig. 4. The SEM images of T-ZnO (A), pads II (B) and III (C).

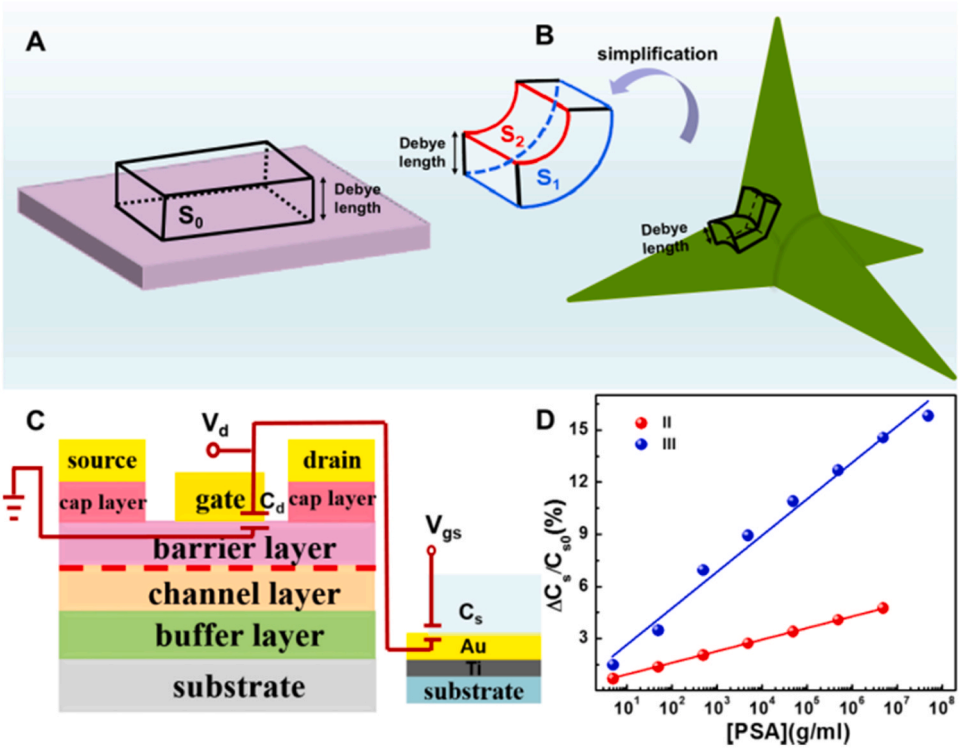

Fig. 5. Schematic diagram of Debye volume belonging to the flat Au surface(A) and T-ZnO surface (B). Equivalent circuit of SEGFET biosensor (C). The rate of Cs change for different [PSA] of the pad II and III (D).

evaluate the screening effect of complex detection front, researchers introduced a concept of Debye volume which can be roughly defined as the volume of electrolyte within one Debye length away from the electrode [15,18]. Figs. 5A and 5B is a sketch of Debye volume of the two types of detection fronts in our work, i.e., plane Au and 3D-structure T-ZnO. Here, in order to intuitively understand the Debye volume on the T-ZnO's concave corners, we simplify the T-ZnO's concave corners into a cylindrical concave front. To compare the Debye volume of different detection fronts, it should determine the same surface area of the electrolyte directly contacting with them, herein i.e. S_0 for the plane Au and S_1 for the cylindrical concave front. Due to a smaller area of the upper surface (S_2), the Debye volume belonging to the cylindrical concave front is smaller than that of a flat Au one. A smaller Debye volume implies a smaller amount of counter ions filling in it, and consequently weaker screening effect. This is also consistent with the simulation results of the potential distribution on the concave surface reported in previous literature [18], that is, the concave front has a smaller potential change compared with the plane and the convex ones and therefore has a larger equivalent Debye length. The electrolyte environment at the concave corner of the T-ZnO is comparable to that of the cylindrical concave front with a large curvature, and hence has a small Debye volume. Specially, each T-ZnO with a four-legs structure has several concave corners and provides abundant high-sensitivity detection fronts, hence is a promising modification material for the sensing pad. As shown in Fig. 3, both biosensors II and III (with T-ZnO) show clear improvement in *S* compared with biosensors I. For the physical modification scheme (biosensor II), the probes are prone to lying on the upturned concaves only. For the chemical bio-functionalization method (biosensors III), APTES and glutaraldehyde can help the probes to be also fixed on the lateral concaves even bottom ones. Thus, it's reasonable that biosensors III have larger *S* than biosensors II. In a word, more biological signals can be detected by the transistor when the sensing pad is modified with T-ZnO nanostructures with many concave corners, consequently promoting the detection sensitivity.

In order to further discover why biosensor III shows the optimal sensitivity, we should first clarify the working mechanism of our SEGFET biosensor. Its equivalent circuit is shown in Fig. 5C. When the gate bias (V_g) is applied by the reference electrode, the surface of pad will form an electrical double layer capacitance (C_s) which is in series with the HEMT device capacitance (C_d), thus, the potential drop across the transistor (V_d) can be expressed by [32]:

$$V_d = \frac{C_s}{C_d + C_s} \times V_g \tag{4}$$

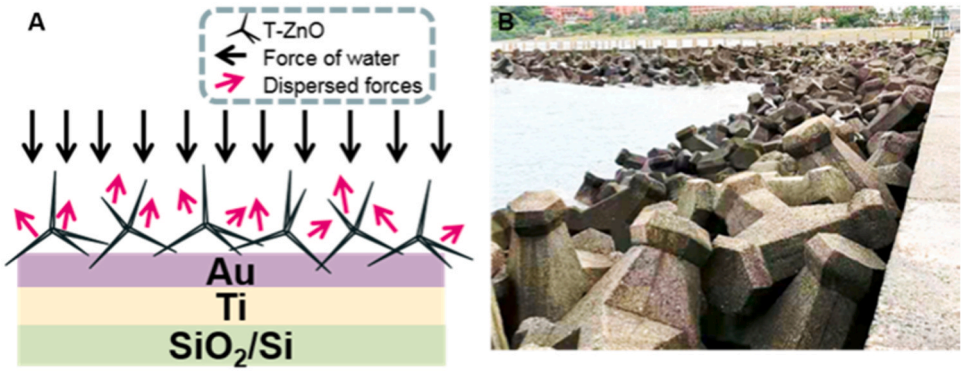

Fig. 6. Schematic diagram of the process by which T-ZnO disperses the stress effect of water (moisture) on the Au film (A). Imagine of seawall and armor blocks (B).

It can be seen from the formula that V_d will be affected by C_s. The relative capacitance changes ($\Delta C_s/C_{s0}$, where ΔC_s refers to the difference between the C_s at a certain [PSA] and in the pure 0.1 × PBS solution C_{s0}) of the pads II and III are shown in Fig. 5D, demonstrating a linear increase with [PSA] in logarithmic coordinates. The pad III has a relatively higher C_s change, up to 10.9% at 50 pg/ml PSA, while only 3.4% for the pad II. This implies a larger V_g response for biosensor III to the same [PSA] according to Eq. (1), consequently better sensitivity. And the capacitance variation difference between the two kind of biosensors may be attributed to the different geometric configuration of biomolecule distribution on the sensing pad. The charge density of many biomolecules (such as dsDNA), has been reported to be at least one order of magnitude higher than physiological salt concentration [33,34]. Consequently, it is suggested that the spatial distribution of anti-PSA and PSA can effectively affect the state of charge distribution around them and then the C_s value. As shown in Fig. 4, both the top and bottom leg of T-ZnO on the pad III can attract the anti-PSA, while only at the bottom leg on the pad II. This implies that both the amount and geometric distribution of biological charges are different between the two types of pads. More biological-binding sites and more abundant geometric distribution of them are available for the pad III, which makes it possess stronger capacitance regulation ability and then higher sensitivity compared with the pad II.

In the literatures, FET-based biosensors generally adopted plane Au films as the detection front like strategy I in our work, but the stability issue was rarely focused on. As we know, the adhesion strength between Au and the frequently-used substrates is not satisfying, which would affect the conductivity and stability of Au films, and then the biosensor stability. In our experiment, we do observe that the Au film was peeled off from the SiO_2/Si substrate when exposed to an ambient atmosphere with high temperature and humidity in the summer. Consequently, in solution environment, most of bare Au pads (although with good appearance) present large resistance and capacitance variations during repeating tests, and their corresponding biosensor-like device (without anti-PSA probes) also has fluctuant current and threshold voltage (Fig. S4). So, it's logically believed that pads I-based biosensors are with stability issues (Fig. 2). But fortunately, by covering T-ZnO nanostructures, both the sensing pads and biosensors demonstrate greatly-improved stability. And the detachment of Au films from the substrate never occurs again. It's proposed that the T-ZnO on Au surface can serve as a 'protective cover', in analogy with armor blocks around the seawall [35]. The seawall is usually filled with irregular stones (i.e. armor blocks) which can effectively disperse the impact stress of the sea waves and then reduce the damage to the seawall (Fig. 6A). Similarly, T-ZnO can release the stress effect of water (moisture) on the Au film (Fig. 6B) and consequently improve the stability. In addition, the hydrophilicity of the bare and the T-ZnO-modified Au pads were also examined, with a contact angle of 75.67° and 69.97°, respectively (The contact angle was measured using dynamic contact angle meter (DCAT21, Data physics, Germany) with a DI water droplet, as shown in Fig. S5a). In fact, oxide materials including T-ZnO with hydrophilicity are prone to absorbing moisture in air, which helps to reduce the erosion of the Au film against water. Thus, the introduction of T-ZnO can effectively improve the stability of SEGFET, which is helpful to broaden the process window for the preparation of sensing pad and improve the yield rate of devices.

4. Conclusions

In this report, we constructed a series of SEGFET-configuration biosensors to systematically study the corresponding sensing performance and stability, in which the sensing pads were functionalized by three different strategies. With a common Au film as the sensing pad, the detection performance and stability of the biosensor is undesirable. Through modifying the Au film surface by T-ZnO to form a 3D and concave detection front, the detection scope, sensitivity and stability are greatly improved. Essentially, the reason for the larger detection scope is that 3D-structure T-ZnO can provide more biological modification sites. The improvement in sensitivity is contributed to the weaker Debye screening of the 3D and concave T-ZnO front. And the hydrophilic T-ZnO with a four-leg configuration can effectively release the stress and erosion effect of water (moisture) on the Au film, which helps to improve long-term air stability and test repeatability in bio-solution. In addition, the detection scope and sensitivity are further promoted by applying chemical modification method because it can provide more biological modification sites and greater capacitance regulation ability. It is believed that the optimized functionalizing strategy to construct detection front can become a versatile technology to achieve high-performance FET-based biosensors.

CRediT authorship contribution statement

Jiahuan Yu (First Author) and **Guosheng Gao (Co-first Author):** Conceptualization, Methodology, Software, Investigation, Formal analysis, Writing – original draft; **Bo Sun:** Data curation, Writing – original draft; **Lingyan Liang (Corresponding Author):** Conceptualization, Funding acquisition, Resources, Supervision, Writing – review & editing; **Qiang Shen:** Visualization, Investigation, Resources, Formal analysis; **Yang Zhang (Corresponding Author):** Validation, Writing – review & editing, Funding acquisition, Project administration; **Hongtao Cao (Corresponding Author):** Supervision, Visualization, Funding acquisition, Writing – review & editing.

Declaration of Competing Interest

The authors declare that they have no known competing financial interests or personal relationships that could have appeared to influence the work reported in this paper.

Acknowledgments

The authors gratefully acknowledge financial support from Natural Science Foundation of Zhejiang Province (Grant No. LY20F010002) and Ningbo Public Service Technology Foundation, China (Grant No. 202002N3156).

Appendix A. Supporting information

Supplementary data associated with this article can be found in the online version at doi:10.1016/j.jpba.2022.114597.

References

[1] M. Kaisti, Detection principles of biological and chemical FET sensors, Biosens. Bioelectron. 98 (2017) 437–448.
[2] M.J. Schöning, A. Poghossian, Recent advances in biologically sensitive field-effect transistors (BioFETs), Analyst 127 (2002) 1137–1151.
[3] A. Poghossian, M.J. Schöning, Label-free sensing of biomolecules with field-effect devices for clinical applications, Electroanalysis 26 (2014) 1197–1213.
[4] J. Wang, Electrochemical biosensors: towards point-of-care cancer diagnostics, Biosens. Bioelectron. 21 (2006) 1887–1892.
[5] P. Bergveld, Development of an ion-sentivity solid-state device for neurophysiological measurements, IEEE Trans. Biomed. Eng. BM17 (1970) 70–71.
[6] P. Bergveld, Development, operation, and application of ion-sensitive field-effect transistor as a tool for electrophysiology, IEEE Trans. Biomed. Eng. BM19 (1972) 342–351.
[7] L.T. Yin, J.C. Chou, W.Y. Chung, T.P. Sun, S.K. Hsiung, Study of indium tin oxide thin film for separative extended gate ISFET, Mater. Chem. Phys. 70 (2001) 12–16.
[8] Q. Zhang, H.S. Majumdar, M. Kaisti, A. Prabhu, A. Ivaska, R. Osterbacka, A. Rahman, K. Levon, Surface functionalization of ion-sensitive floating-gate field-effect transistors with organic electronics, IEEE Trans. Electron Devices 62 (2015) 1291–1298.
[9] W.J. Cho, C.M. Lim, Sensing properties of separative paper-based extended-gate ion-sensitive field-effect transistor for cost effective pH sensor applications, Solid State Electron 140 (2018) 96–99.
[10] E.K. Hong, W.J. Cho, High sensitivity In-Ga-Zn-O nanofiber-based double gate field effect transistors for chemical sensing, Sens. Actuators B Chem. 326 (2021) 128827.
[11] N.C.S. Vieira, E.G.R. Fernandes, A.D. Faceto, V. Zucolotto, F.E.G. Guimaraes, Nanostructured polyaniline thin films as pH sensing membranes in FET-based devices, Sens. Actuators B Chem. 160 (2011) 312–317.
[12] N.C.S. Vieira, A. Figueiredo, A.D. Faceto, A.A.A. de Queiroz, V. Zucolotto, F.E.G. Guimaraes, Dendrimers/TiO2 nanoparticles layer-by-layer films as extended gate FET for pH detection, Sens. Actuators B Chem. 169 (2012) 397–400.
[13] L.Y. Liang, S.N. Zhang, W.H. Wu, L.Q. Zhu, H. Xiao, Y.H. Liu, H.L. Zhang, K. Javaid, H.T. Cao, Extended-gate-type IGZO electric-double-layer TFT immunosensor with high sensitivity and low operation voltage, Appl. Phys. Lett. 109 (2016) 173501.
[14] S. Yang, L. Gu, X.Z. Ding, B. Miao, Z.Q. Gu, L.Y. Yang, J.D. Li, D.M. Wu, Disposable gate AlGaN/GaN high-electron-mobility sensor for trace-level biological detection, IEEE Electr. Device L 39 (2018) 1592–1595.
[15] V. Kesler, B. Murmann, H.T. Soh, Going beyond the debye length: overcoming charge screening limitations in next-generation bioelectronic sensors, ACS nano 14 (2020) 16194–16201.
[16] M. Kaisti, Detection principles of biological and chemical FET sensors, Biosens. Bioelectron. 98 (2017) 437–448.
[17] W. Huang, A.K. Diallo, J.L. Dailey, K. Besar, H.E. Katz, Electrochemical processes and mechanistic aspects of field-effect sensors for biomolecules, J. Mater. Chem. C. 3 (2015) 6445–6470.
[18] K. Shoorideh, C.O. Chui, On the origin of enhanced sensitivity in nanoscale FET-based biosensors, Proc. Natl. Acad. Sci. U. S. A. 111 (2014) 5111–5116.
[19] N. Gao, W. Zhou, X. Jiang, G. Hong, T.M. Fu, C.M. Lieber, General strategy for biodetection in high ionic strength solutions using transistor-based nanoelectronic sensors, Nano Lett. 15 (2015) 2143–2148.
[20] N. Gao, T. Gao, X. Yang, X. Dai, W. Zhou, A. Zhang, C.M. Lieber, Specific detection of biomolecules in physiological solutions using graphene transistor biosensors, Proc. Natl. Acad. Sci. U. S. A. 113 (2016) 14633–14638.
[21] M.K. Xu, S.F. Li, M. Guan, Y. Zhang, Y.P. Zeng, Extended-gate AlGaAs/GaAs HEMT for accurate cardiac troponin I antigen detection in clinical human serum, Appl. Phys. Express 13 (2020) 021003.
[22] J.D. Li, J.J. Cheng, B. Miao, X.W. Wei, J. Xie, J.C. Zhang, Z.Q. Zhang, D.M. Wu, Detection of prostate-specific antigen with biomolecule-gated AlGaN/GaN high electron mobility transistors, J. Micromech. Microeng. 24 (2014) 075023.
[23] J. Zhou, N.S. Xu, Z.L. Wang, Dissolving behavior and stability of ZnO wires in biofluids: a study on biodegradability and biocompatibility of ZnO nanostructures, Adv. Mater. 18 (2006) 2432–2435.
[24] F. Zhang, X. Wang, S. Ai, Z. Sun, Q. Wan, Z. Zhu, Y. Xian, L. Jin, K. Yamamoto, Immobilization of uricase on ZnO nanorods for a reagentless uric acid biosensor, Anal. Chim. Acta 519 (2004) 155–160.
[25] Y. Gu, J. Zhou, W. Mai, Y. Dai, G. Bao, Z.L. Wang, Measuring the transport property of ZnO tetrapod using in situ nanoprobes, Chem. Phys. Lett. 484 (2010) 96–99.
[26] Y. Song, X. Zhang, X. Yan, Q. Liao, Z. Wang, Y. Zhang, An enzymatic biosensor based on three-dimensional ZnO nanotetrapods spatial net modified AlGaAs/GaAs high electron mobility transistors, Appl. Phys. Lett. 105 (2014) 213703.
[27] J.H. Yu, M.K. Xu, L.Y. Liang, M. Guan, Y. Zhang, F. Yan, Separative extended-gate AlGaAs/GaAs HEMT biosensors based on capacitance change strategy, Appl. Phys. Lett. 116 (2020) 123704.
[28] G. Ertürk, H. Özen, M.A. Tümer, B. Mattiasson, A. Denizli, Microcontact imprinting based surface plasmon resonance (SPR) biosensor for real-time and ultrasensitive detection of prostate specific antigen (PSA) from clinical samples, Sens. Actuators B Chem. 224 (2016) 823–832.
[29] M.Y. Shen, B.R. Li, Y.K. Li, Silicon nanowire field-effect-transistor based biosensors: from sensitive to ultra-sensitive, Biosens. Bioelectron. 60 (2014) 101–111.
[30] B.M. Lowe, K. Sun, I. Zeimpekis, C.K. Skylaris, N.G. Green, Field-effect sensors-from pH sensing to biosensing: sensitivity enhancement using streptavidin–biotin as a model system, Analyst 142 (2017) 4173–4200.
[31] J. Zhou, N.S. Xu, Z.L. Wang, Dissolving behavior and stability of ZnO wires in biofluids: a study on biodegradability and biocompatibility of ZnO nanostructures, Adv. Mater. 18 (2006) 2432–2435.
[32] C.H. Chu, I. Sarangadharan, A. Regmi, Y.W. Chen, C.P. Hsu, W.H. Chang, G.Y. Lee, J.I. Chyi, C.C. Chen, S.C. Shiesh, G.B. Lee, Y.L. Wang, Beyond the Debye length in high ionic strength solution: direct protein detection with field-effect transistors (FETs) in human serum, Sci. Rep. 7 (2017) 5256.
[33] H. Long, A. Kudlay, G.C. Schatz, Molecular dynamics studies of ion distributions for DNA duplexes and DNA clusters: salt effects and connection to DNA melting, J. Phys. Chem. B 110 (2006) 2918–2926.
[34] C.P. Hsu, Y.F. Huang, Y.L. Wang, Investigation of the non-faradaic current of DNA-immobilized microelectrodes in concentrated salt environment for biosensors, ECS J. Solid State Sc. 5 (2016) Q149–Q154.
[35] A. Chow, T. Leung, F. Lee, Benefit–cost analysis on coastal structures design for climate change adaptation in Hong Kong, Coast. Eng. J. 59 (2017) 1740005.